Multifunctional Ferrofluid-Infused Structured Surfaces with Dynamically Reconfigurable Multiscale Topography

Wendong Wang[†1,2,3], Jaakko V. I. Timonen[†1,4], Andreas Carlson[1,2,5], Dirk Drotlef[3], Cathy T.Y. Zhang[1,2], Stefan Kolle[1], Alison Grinthal[1], Tak-Sing Wong[1,2], Benjamin Hatton[1,2], Sung Hoon Kang[1,2], Stephen Kennedy[1,2], Joshua Chi[1,6], Robert Thomas Blough[2], Metin Sitti[3], L. Mahadevan[1,2,7], Joanna Aizenberg[1,2,6,7]*

[1]John A. Paulson School of Engineering and Applied Sciences, Harvard University, Cambridge, Massachusetts 02138, USA. [2]Wyss Institute for Biologically Inspired Engineering, Harvard University, Cambridge, Massachusetts 02138, USA. [3]Max Planck Institute for Intelligent Systems, Stuttgart, 70569, Germany. [4]Department of Applied Physics, Aalto University School of Science, Espoo FI-02150, Finland. [5]Department of Mathematics, Mechanics Division, University of Oslo, 0851 Oslo, Norway. [6]Department of Chemistry and Chemical Biology, Harvard University, Cambridge, Massachusetts 02138, USA. [7]Kavli Institute for Bionano Science & Technology, Harvard University, Cambridge, Massachusetts 02138, USA.

Developing adaptive material systems whose geometries change in response to external stimuli not only generates fundamental insights into the relationship between the shape-altering physical forces and the resulting morphologies, but also has immense technological relevance in areas from creating dynamic interfaces with biological tissues to designing energy-efficient aircrafts[1,2]. In particular, reconfigurable surface topography has been designed using responsive gels[3], shape-memory polymers[4], liquid crystals[5-7], or hybrid composites[8-13] through biomimetic approaches to control interfacial properties[14]. The resulting functions of these existing designs are restricted by the limited types of their structure-specific topographical changes. Here we show a hierarchical magneto-responsive composite surface made by infiltrating an active component—ferrofluid—into a passive microstructured matrix (so-called ferrofluid-containing liquid-infused porous surfaces—FLIPS), and demonstrate unique topographical reconfigurations at multiple length scales and a broad range of associated emergent behaviours. The magnetic field induces the movement of nanoscopic magnetic nanoparticles, which leads to microscopic flow of ferrofluid first above and then within the microstructured surface. This redistribution changes the initially smooth surface of the ferrofluid immobilized by the porous matrix through capillary force, into various multiscale hierarchical topographies shaped by the size, arrangement and orientation of the confining microstructures in the magnetic field. We provide detailed theoretical and experimental analyses of the spatial and temporal dynamics of these reconfigurations based on the balance between capillary and magnetic pressure[15-19] and geometrical anisotropy of the FLIPS system. A number of interesting functions at three different length scales are demonstrated: at micron-scale, manipulation and self-assembly of colloidal particles; at millimeter scale, flow control of liquid droplets; at centimeter scale, switchable adhesion and friction, liquid pumping, and removal of biofilms. We envision that FLIPS can be developed into an integrated platform for exploring and designing control systems for manipulation and transport of matter, thermal management, microfluidics, and fouling-release materials.

While the magnetic field-induced reconfiguration of a ferrofluid to form macroscopic protuberances on a flat surface is well known[15,16], we anticipated that ferrofluid's behaviour in the microstructured confinement may elicit a range of otherwise unachievable multiscale topographical responses enabled by the capillary pressure within the porous substrate (**Fig. 1a**). To explore this concept, we used a variety of microstructured substrates (see Table 1) infiltrated with fluorocarbon- or silicone oil-based ferrofluid. The spatiotemporal changes in surface topography occurring upon application of a magnetic field were visualized using an angled illumination technique, the thickness of the ferrofluid overlayer was measured using a force probe (see **Extended Data Fig. 1**) and the evolution of the profile of the ferrofluid-air interface was measured using a laser scanning microscope (**Extended Data Fig. 2a,b**).

Table 1. Structured surfaces used in this study

Pattern #	Pattern type	Dimensions (μm)
1	Array of microchannels	dx=0; dy=38; h_0=34
2	Array of microchannels	dx=0; dy=38; h_0=15
3	Array of microchannels	dx=0; dy=76; h_0=34
4	Array of microplates	dx=5; dy=38; h_0=30
5	Array of microposts	dx=1.4; dy=1.4; h_0=10
6	Spirally-shaped channels	dx=0; dy=38; h_0=15
7	Microporous membrane	Average pore size = 1
8	Microporous membrane	Average pore size = 10
9	Microporous membrane	Average pore size = 20
10	Microporous tubing	Average pore size = 5-60

The non-uniform magnetic field created by a magnet below FLIPS initiates three sequential and interrelated processes to generate dynamic multiscale topographies (**Fig. 1b**). In the first step, the magnet starts to withdraw the initially flat ferrofluid overlayer. Withdrawal leads to the formation of a macroscopic protuberance with lateral size comparable to that of the magnet (ca. 1 - 20 mm). In the second step, the ferrofluid that remains trapped in the porous matrix through capillary force is pulled out of the pores by a magnetic pressure $|p_m| \approx \mu_0 M_s H_0$ (**Extended Data Fig. 3a-c**), where μ_0 [N·A^{-2}] is the vacuum permeability, M_s [A·m^{-1}] the saturation magnetization of the ferrofluid, and H_0 [A·m^{-1}] the strength of the applied magnetic field[15]. The magnetic pressure is counteracted by the capillary pressure $p_\gamma \approx 2\gamma/dy$, where γ is the surface tension of the ferrofluid-air interface and $dy/2$ is half of the width of the channels and the largest characteristic radius of the porous matrix. If $|p_m| \leq p_\gamma$, ferrofluid will remain trapped in the pores (**Extended Data Fig. 3e-g**). If $|p_m| > p_\gamma$, such as the case shown in **Fig. 1b** and **Extended Data Fig. 3d**, where $|p_m| \approx 10^4$ Pa and $p_\gamma \approx 10^3$ Pa, ferrofluid will be extracted from the pores, leading to the appearance of the conformally-coated micro-topographic region *1*. In the third step, the micro-topographical area expands outwards through porous-capillary flow, while the macroscopic protuberance continues to grow through the accumulation of ferrofluid. The initial extraction of ferrofluid from the areas around the magnet deforms the ferrofluid-air interface. This interface deformation induces a capillary force along the microstructures, even in areas far from the magnet where the magnetic pressure is smaller than capillary pressure. Over time, the interface has a gradually increasing height along the channel, from its minimum near the magnet to its maximum height h_0 in the far field (**Fig. 1c** and **Extended Data Fig. 2b**). The combination of the magnetic suction force and the capillary force makes the flow follow the micro-topography, even in highly complex channel geometries such as a spiral shape of pattern #6, where the flow makes turns along a curved path (see **Extended Data Fig.2e)**.

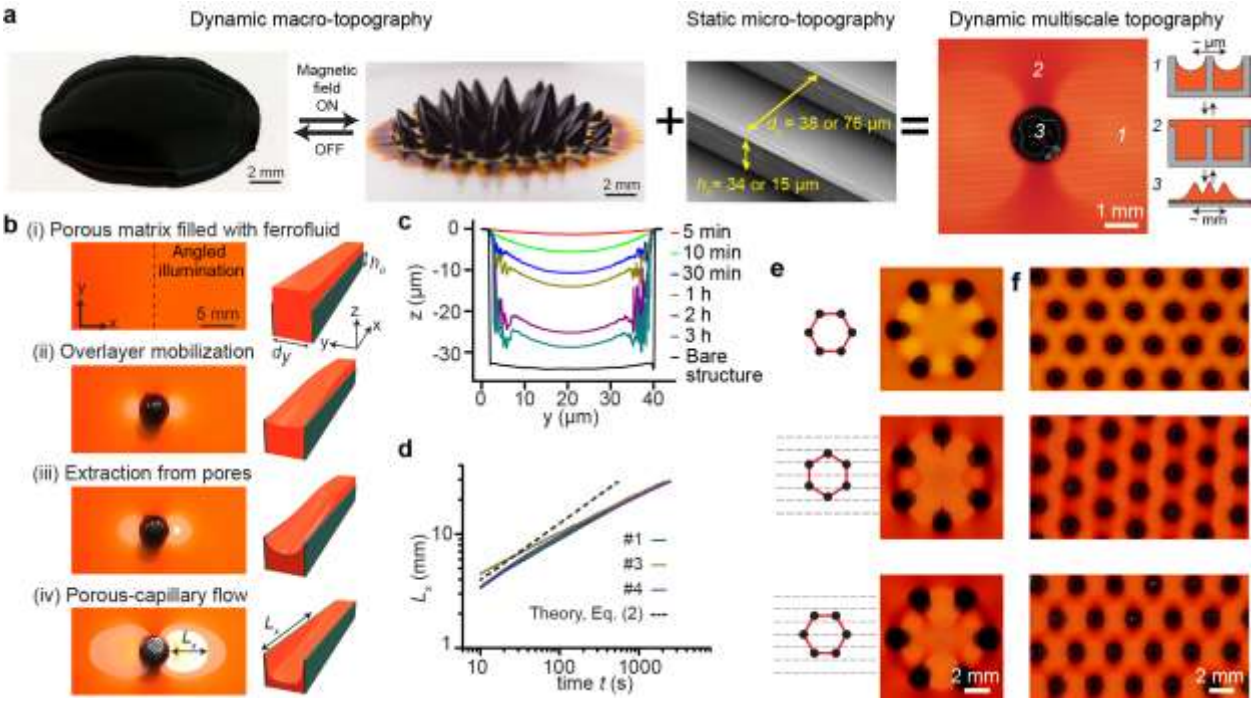

Figure 1. Dynamic multiscale topography of ferrofluid-containing liquid-infused porous surface (FLIPS). (a) A diagram showing the concept of FLIPS. Left: Two topographic states of a ferrofluid spreading on an unstructured surface, depicting the transformation from the flat interface to macroscopic protuberances in response to an external magnetic field. Middle: Scanning electron micrograph (SEM) of the static micro-topography of exemplary microchannel substrates #1-3 (see **Table 1**). Right: Top view photo of FLIPS under magnetic field, showing that the ferrofluid confined within the microstructured solid experiences unique, area-selective topographical reconfigurations at multiple length scales: region *1* exhibits micro-topography shaped by the structured substrate; region *2* exhibits a flat surface, and region *3* exhibits the macro-topographical protuberance. **(b)** Transport processes involved in the formation of macro- and micro-topographical features: the left column shows a series of representative experimental photos in top view captured using the angled illumination technique (see **Extended Data Fig. 1b**); the right column shows the corresponding schematics depicting the deformation of the ferrofluid-air interface in a microchannel. **(c)** Evolution of cross-section profiles of ferrofluid-air interface at a fixed distance (~ 1.5 cm away from the magnet) over time measured using a laser scanning microscope. **(d)** The log-log plots of experimentally measured L_x versus time t for surfaces #1, 3, 4 from Table 1. The dashed black line is plotted according to equation (2), with γ = 17 mN/m, η = 0.367 Pa.s and h_0 = 34 µm. See **Supplementary Video 1** for a representative movie showing the spatiotemporal evolution of the multiscale topography. The overlayer thicknesses are ~10–20 µm. **(e-f)** Multiscale topographical response to a hexagonal pattern of six (e) or more (f) magnets (diameter 1.6 mm, magnet spacing 3.2 mm): the top row shows the case without the microstructured substrate; the bottom two rows show the cases with the microstructured substrate #4 but different orientation of the hexagonal pattern. See **Supplementary Video 1**.

The size of the micro-topographical area, characterized by L_x, was observed to scale with time as $L_x \sim t^{0.35–0.5}$ for different patterns and overlayer dimensions tested **(Fig. 1d** and **Extended Data Fig. 2c,d**). By balancing the rate of change of work done by the capillary force with the viscous dissipation, we obtain

$$\left(\gamma \dot{L_x} d_y\right) \approx \gamma d_y U \approx \int \eta \left(\frac{\partial U}{\partial z}\right)^2 dV \approx \eta \left(\frac{U}{h_0}\right)^2 h_0 L_x d_y, \quad (1)$$

Where $U \approx \dot{L_x}$ and $\dot{L_x} = dL_x/dt$. Rearranging the terms and integrating with respect to time t gives a scaling relation for L_x that correlates well with the experimental data:

$$L_x(t) \approx \left(\frac{\gamma h_0}{\eta}\right)^{1/2} \cdot t^{1/2}, \quad (2)$$

where γ is the surface tension; η is the dynamic viscosity; h_0 is the height of the microstructure. The magnetic pressure $|p_m|$ generates a force on the ferrofluid, where an alternative derivation to the scaling relationship (2) is obtained by replacing the left hand side of (1) by the rate of change of work done by the magnet on the ferrofluid $\left(|p_m|\dot{L_x} d_y h_0\right)$ and integrating with respect to time:

$$L_x(t) \approx \left(\frac{|p_m| h_0^2}{\eta}\right)^{1/2} \cdot t^{1/2}. \quad (3)$$

Both derivations give the same power law dependence with respect to time $L_x \sim t^{1/2}$ and only differ in pre-factors. Despite their simplicity, these scaling relations provide a reasonable order-of-magnitude approximation to describe the dynamics revealed in the experimental data. They also capture the dependence of L_x on h_0 and the independence of L_x from d_x and d_y. The discrepancy between the experiments and these scaling laws may be due to the three-dimensional shape of the microchannels, the complex shape of the ferrofluid-air interface and the dependence on the thickness of the ferrofluid overlayer (see **Extended Data Fig. 2c**) that the current models do not fully capture.

The asymmetry of the microchannels used in the demonstrations above induces preferential asymmetric extraction of the ferrofluid from the channels along the x-direction and the appearance of the characteristic dumbbell-shaped micro-topographical signature (**Supplementary Video 1)**. Additional length scales can be introduced by using patterned or structured magnetic fields applied to geometrically anisotropic FLIPS. Such fields can be created by organizing multiple permanent magnets into an array. For example, a hexagonal cluster of six magnets acting on a FLIPS with a channel-like array of microplates introduces one more symmetry element to the system, leading to more complicated flow patterns that reflect the relative orientation of the anisotropic microstructures in the patterned magnetic field (**Fig. 1e**). Since the field source is no longer axisymmetric, the orientation of the field source (6-fold rotational symmetry) with respect to the microplates (2-fold rotational symmetry) allows for one more degree of control over the topographical response (**Fig. 1e** and **Supplementary Video 1**), with the opportunities to be expanded to any combination of the magnet assembly (e.g., "infinite" arrays of magnets, see **Fig. 1f**) and the structured surface.

The FLIPS concept introduced here offers unprecedented versatility and modularity in designing dynamic surfaces with multiscale topographical responses. In the examples shown above and below, we demonstrate that the specific topographical patterns can be finely tuned by controlling (i) the properties of the ferrofluid (e.g. concentration and type of magnetic particles or the type and viscosity of the carrier fluid); (ii) the geometry of the microstructured substrate; (iii) the strength and the pattern of the magnetic field; and (iv) the relative orientation and distance of the FLIPS from the magnets. The resulting spatial and temporal dynamics of topographical reconfiguration enable numerous functions at multiple length scales.

At the micron scale, FLIPS offers a new approach for manipulation of colloidal matter on 2D interfaces (**Fig. 2**). Depending on the state of the dynamic topography, colloidal particles can form a disordered 2D gas-like state (on flat topography, **Fig. 2a**) or organize into structures such as chains (on micro-topographic regions, **Fig. 2b**). Subsequently, FLIPS allows for controlled

transport of non-magnetic colloids when a horizontal body force on the ferrofluid is exerted by a lateral magnetic field gradient (**Fig. 2c,d**). The transport mechanism is unique, as it does not correspond to either positive or negative magnetophoresis of magnetic colloidal matter that have been studied extensively before[20]. Instead, the force on the non-magnetic particle is created hydrodynamically by coupling of the ferrofluid flow under the field gradient to the motion of the aqueous phase on top of the ferrofluid (**Fig. 2e**). Under typical experimental conditions utilizing small permanent magnets as field sources, the speed of the colloids is on the order of a few μm/s and controllable with the magnetic field (**Fig. 2f and Supplementary Video 2**).

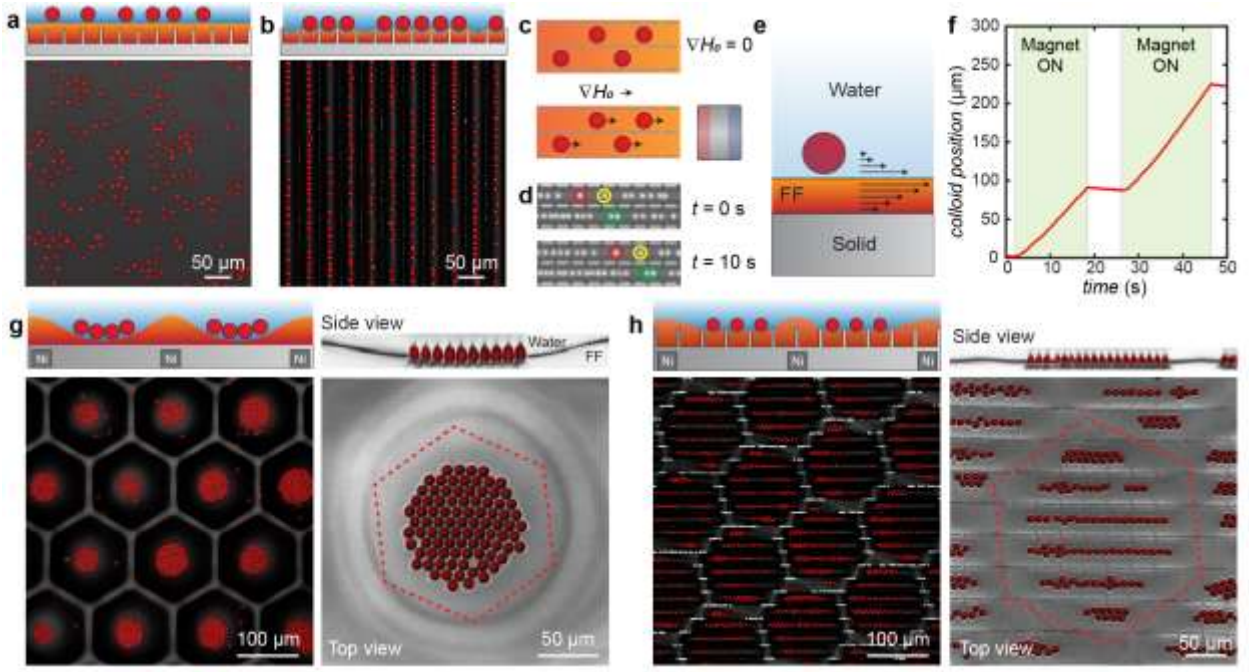

Figure 2. Applications of FLIPS at the micron scale: manipulation of non-magnetic colloidal particles on FLIPS. **(a-b)** Schematic and confocal fluorescence images of 10 μm melamine colloidal particles floating on the flat surface of FLIPS in the absence of a magnetic field (a) and confined in micro-topography of FLIPS when ferrofluid has been locally depleted from the microstructures with a magnet (b). **(c)** Schematics showing colloidal particles staying stationary in the absence of a magnetic field gradient (top) and moving in the presence of a magnetic field gradient (bottom). **(d)** Optical images showing the transport of colloidal particles along the micro-topographical region. Four particles are labelled to depict their movement within a 10s interval. See **Supplementary Video 2**. **(e)** Schematic illustrating the mechanism behind the transport of non-magnetic colloidal particles in a magnetic field: the transport of ferrofluid induces a flow of water near the ferrofluid-water interface, and this induced water flow moves the colloidal particles. **(f)** Plot of colloidal position vs. time. **(g-h)** Schematic and confocal fluorescence images showing the confinement of colloidal particles by the macro-topographical response of a thin layer of ferrofluid alone (without micro-topography) (g) and the confinement of colloidal particles by the macro- and micro-topographical response of FLIPS (h). A hexagonal nickel grid embedded in FLIPS is used to shape a nearly uniform external magnetic field into a hexagonally varying field intensity pattern.

Multiscale topography can also be used for assembling colloidal matter into otherwise inaccessible hierarchical structures. For example, in the case of ferrofluid alone, a hexagonal soft ferromagnetic nickel grid leads to the formation of a hexagonally varying periodic ferrofluid pattern on which colloidal particles assemble into close-packed clusters (**Fig. 2g**), whereas in the

case of FLIPS, a multiscale topographical response is created, and colloidal matter organizes into short line segments as dictated by the two symmetries (**Fig. 2h**).

At the millimeter scale, FLIPS can be harnessed for controlling the motion, clustering, and interaction of liquid droplets. We use gravitational force to drive the flow of droplets on a tilted FLIPS, and tune the multiscale topographical response by adjusting the magnetic field strength and gradients through varying the distance, *d*, between the magnet and FLIPS (**Fig. 3a**). On one hand, the reversible appearance of micro-topography creates switchable slippery surfaces[21] that pin the droplets at micro-topographic regions or release the droplets when the magnetic field strength is reduced to remove the micro-topography (**Fig. 3b**, **Supplementary Video 3**). On the other hand, the macro-topographical protuberance can be used for assembling droplets into well-defined clusters (**Fig. 3c**). To demonstrate this unique behavior, we note that when a droplet slides near the protuberance, it is pinned to it by capillary and magnetic forces. Subsequent droplets will enter the trap and combine with the previously pinned droplets to form clusters, until their collective gravity overcomes their attraction to the protuberance. Then they are released as doublets, triplets, quadruplets, or quintuplets, depending on the adhesion controlled by the distance between the magnet and the FLIPS (**Supplementary Video 4**). If the droplets contain polymerizable moieties, these clusters can be solidified into distinct assemblies.

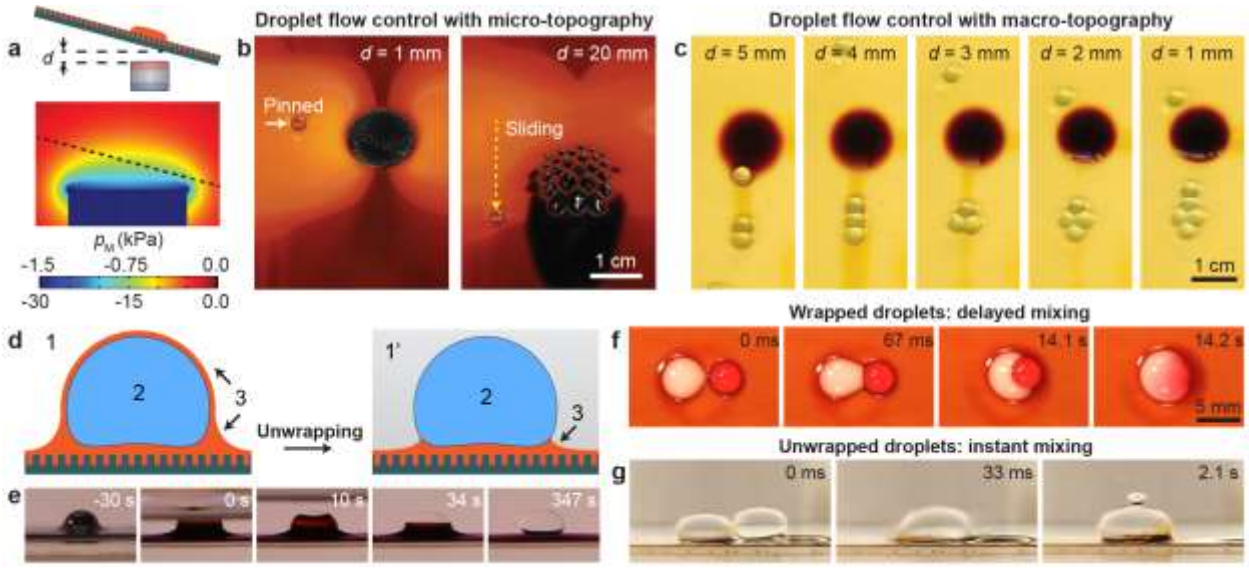

Figure 3. Applications of FLIPS at the millimeter scale: droplet flow control and droplet manipulation. (a) Top: Schematic showing the configuration of experimental set-up in (b) and (c). FLIPS is tilted and placed above the magnet. The distance *d* between the magnet and FLIPS can be varied. Bottom: Simulated graph of the magnetic pressure distribution around the magnet. The upper and lower scales of the legend for the magnetic pressure distribution correspond to (c) and (b), respectively. **(b)** Two photographs showing a water droplet pinned on the micro-topographical area and its subsequent release after the magnet was lowered to allow ferrofluid to flow back and submerge the micro-topography. See **Supplementary Video 3**. **(c)** Five photographs showing different clustering behaviours of 15 μL water droplets on the macro-topographical feature at five different *d*'s. This FLIPS used diluted ferrofluid and hence did not have a micro-topographical area (see **Extended Data Fig. 3e**). See also **Supplementary Video 4**. (**d**) Schematic showing the unwrapping of a thin ferrofluid layer around a water droplet by changing the surrounding medium from air to a hydrocarbon. The three phases are 1-air, 1'-a hydrocarbon, 2-water, and 3-ferrofluid. (**e**) Five photographs showing the unwrapping of a thin layer of ferrofluid around a water droplet after the addition of dodecane. See **Supplementary Video 5**. (**f**) Four photographs showing

the delayed mixing of two liquid droplets in the presence of wrapping layers. The white droplet is the suspension of 10 μm polystyrene colloids in ethanol, and the red droplet is the suspension of 10 μm polystyrene colloids in water dyed with Rhodamine B. They were brought together by a stationary alternating current (AC) electromagnet at the center beneath the FLIPS. **(g)** Three photographs showing instant mixing of two droplets in the absence of wrapping layers. The left droplet is an aqueous solution of sodium bicarbonate, and the right droplet is an aqueous solution of 2M hydrochloric acid. The right image shows the CO_2 bubble formed as a result of the droplets' coalescence. See **Supplementary Video 6**.

Another droplet manipulation strategy involves the control over the formation of the ferrofluid wrapping layer around the droplets. For example, by replacing air with an alternative liquid medium that is immiscible with the ferrofluid or the droplets, such as a hydrocarbon, the non-transparent ferrofluid wrapping layer around the water droplets can be removed (**Fig. 3e** and **Supplementary Video 5)**. The unwrapping can be used to accelerate the coalescence of droplets: compared with the wrapped droplets with the mixing delayed by >10 s (**Fig. 3f**), the unwrapped droplets mix instantaneously (**Fig. 3g** and **Supplementary Video 6)**, allowing for rapid initiation of chemical reactions. (We note that while existing theory suggests that the formation of a wrapping layer is due to a positive spreading coefficient[11,22], we found that long range van der Waals interaction is likely to be the decisive force in determining the presence or absence of the wrapping layers; see detailed discussion in **Supplementary Section III** and **Extended Data Tables 1-4** and **Figs 4-5**)[23-25].

Finally, we illustrate the versatility of FLIPS at the centimeter scale by demonstrating their functions in switchable adhesion and friction, liquid pumping, and biofilm removal. We measure the adhesion between FLIPS and another surface by first pressing the test surface against FLIPS and then lifting it. With the field on, deforming the macroscopic protuberances and driving the ferrofluid back into the porous matrix requires external work. Conversely, from an energy viewpoint, the formation of the macroscopic protuberance is favored and can spontaneously open a gap between FLIPS and test surface, which enables switchable adhesion (**Fig. 4a, Supplementary Video 7, and Extended Data Fig. 6a-c**) and friction (**Supplementary Video 8**). Notably, in contrast to traditional ferrofluid-coated unstructured surfaces, FLIPS display area-specific adhesion and friction: regions with flat ferrofluid, with macrostructured protuberances and micro-topography have characteristically different values (**Extended Data Fig. 6d-h**). Furthermore, anisotropic geometry and arrangement of microstructures introduce directionality to friction that can be magnetically controlled (**Extended Data Fig. 6i**) to create unique tunable anisotropic friction materials.

Secondly, by coupling magnets' ability to extract ferrofluid from microporous structures and the movement of the magnets, we demonstrate pumping liquids at centimeter scale (**Fig. 4b** and **Supplementary Video 9**). We infused a porous polytetrafluoroethylene (PTFE) tube with ferrofluid to form a FLIPS pipe. A stepper motor moves five pairs of magnets in circular motion. The ferrofluid between each pair of magnets moves as the magnets rotate and push the test liquid along the tube. The porosity of the PTFE tube wall allows the ferrofluid to follow the circular motion of the pairs of magnets, resulting in continuous pumping enabled by a simple rotation without any complex sequential movement of magnets described earlier[26]. Lastly, using biocompatible fluorocarbon-based ferrofluid, we demonstrate biofilm removal on FLIPS (**Fig. 4c**). We cultured the algae biofilm on FLIPS under quiescent conditions for about a week, and then

moved a magnet under FLIPS and used the macroscopic protuberance to disrupt the green algae biofilm and detach it from the surface (**Supplementary Video 10**).

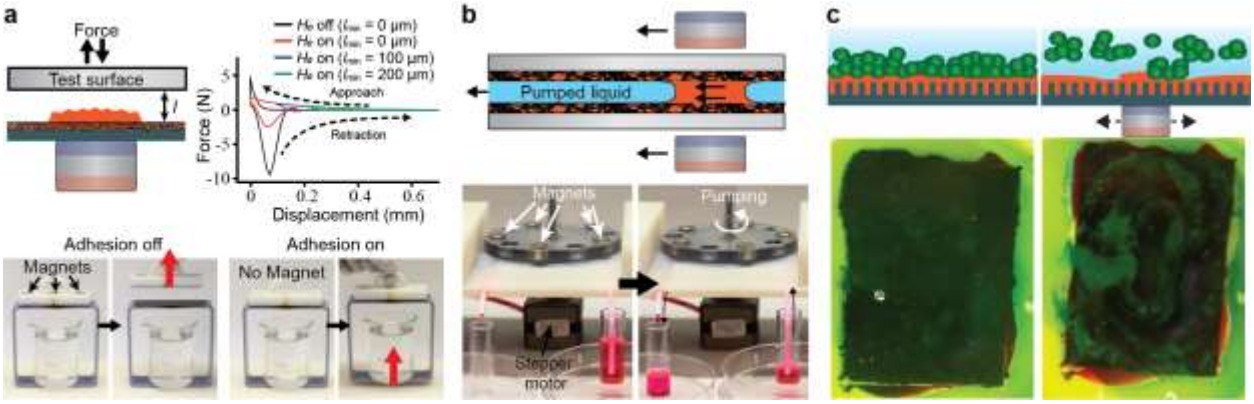

Figure 4. Applications of FLIPS at the centimeter scale: adhesion, pumping, and biofilm removal. (a) Adhesion: The top left schematic shows the setup for adhesion measurement. The test surface is brought in contact with FLIPS at a speed of 0.1 mm/s, held still for 10 s, and then lifted at 1 mm/s. An example of the resulting force vs distance curve is shown on the top right. The test surface in this example is a smooth PTFE. The photographs at the bottom demonstrate switchable adhesion. See **Supplementary Video 7**. **(b)** Pumping: the top is the schematic of the pumping mechanism. The pair of magnets moves the ferrofluid plug along the FLIPS pipe, which in turn drives the liquid (blue) flow inside the pipe. The bottom photographs show that an ethanol solution of Rhodamine B is pumped from the right vial to the left vial. See **Supplementary Video 9**. **(c)** The green algae biofilm is removed by swirling a magnet under FLIPS. Note that the ferrofluids used in these experiments are not toxic (See **Supplementary Section I(I)** and **Video 10)**.

The multiscale topographical response of FLIPS not only possesses intriguing spatial and temporal fluid dynamics features by itself but also provides a wide range of interesting phenomena and novel functions when interfaced with other solids and liquids. Our results suggest that FLIPS allows much more diverse combinations of functional capabilities than surfaces having only a simple, single-scale topographical response[11-13]. The demonstrated applications—new forms of reversible, hierarchical colloidal self-assembly, manipulation and transport of non-magnetic matter in a magnetic field enabled by topography-induced hydrodynamic forces, controlled formation of droplet clusters of well-defined size, switchable adhesion and droplet motion—are only a small representative subset of these capabilities. We emphasize the broad customizability of the FLIPS topographical reconfigurations that can be tuned by changing the magnetic field, ferrofluid and, especially, the geometry and orientation of the confining microstructured surface, which in itself can be made dynamic by using flexible microstructures[8,27]. Our mechanistic insights gained in understanding the governing physical forces in these phenomena and ensuing functions can be readily applied to other technologically relevant developments; for example, to explore the influence of surface topography on turbulent flow[28], to explore the use of the magneto-caloric effect[15] to manage heat transfer with its surrounding system[29], and to explore the minimization of the pump for novel microfluidics platforms[30]. Last but not least, we expect the concept of dynamically reconfigurable multiscale topographies to find uses in biology, such as controlling and stimulating living matter simultaneously at multiple length scales[31,32]. We anticipate that FLIPS and its future developments will benefit such areas as responsive coatings, digital microfluidics, and biological tissue interface with dynamic materials.

Methods Detailed experimental protocols are included in the Supplementary Information file.

Acknowledgements We thank J.C. Weaver for his assistance with 3D printing, M. Khan for his assistance with preparing micro-textured silicon master, P. Kim and J. Alvarenga for their assistance with force measurements, K. Davey at American Electromechanics for his assistance with designing the electromagnet, N. Vogel, I. Morrison, Y. Hu, P. Kim, D. Daniel, M. Kreder, and O. Ahanotu for discussions. W.W. thanks Humboldt foundation for a fellowship. J.V.I.T. was supported by the European Commission through the Seventh Framework Programme (FP7) project DynaSLIPS (project number 626954). This work is supported by DOE under award # DE-SC0005247 (experiment) and by the NSF under award # DMREF-1533985 (theory). This work was performed in part at the Center for Nanoscale Systems at Harvard University (CNS), which is supported by the NSF under award # ECS-0335765.

Author contributions J.A., W.W., and J.V.I.T. designed the experiments. W.W. performed the experiments on dynamics of micro-topography, droplet manipulation and wrapping-layer related calculations, and pumping. J.V.I.T. performed experiments with magnet arrays, and manipulation of colloids. C.T.Y.Z fabricated the microstructures. D.D. measured the ferrofluid overlayer thickness. D.D., M.S. and W.W. performed adhesion and friction measurements. S.Ko. and J.V.I.T. performed biofilm experiments. L.M., A.C., W.W., and J.V.I.T. performed the scaling analysis. A.G. assisted in the design of experiments. S.Ke. and J.C. assisted in droplet experiments. R.T.B. assisted in the pump design. T.-S.W, B.D.H., and S.H.K. contributed to the initial conception of the project. J.A., W.W., J.V.I.T., A.G., and A.C. wrote the manuscript. J.A. supervised the research.

Author information The authors declare no competing conflict of interest. Correspondence and requests for materials should be addressed to J.A. (jaiz@seas.harvard.edu).

References

1 Vaia, R. & Baur, J. Adaptive composites. *Science* **319**, 420-421 (2008).
2 Kuroki, H., Tokarev, I. & Minko, S. Responsive surfaces for life science applications. *Annu. Rev. Mater. Res.* **42**, 343-372 (2012).
3 Yoshida, R. Self-oscillating gels driven by the Belousov-Zhabotinsky reaction as novel smart materials. *Adv. Mater.* **22**, 3463-3483 (2010).
4 Reddy, S., Arzt, E. & del Campo, A. Bioinspired surfaces with switchable adhesion. *Adv. Mater.* **19**, 3833-3837 (2007).
5 van Oosten, C. L., Bastiaansen, C. W. M. & Broer, D. J. Printed artificial cilia from liquid-crystal network actuators modularly driven by light. *Nat. Mater.* **8**, 677-682 (2009).
6 Liu, D., Liu, L., Onck, P. R. & Broer, D. J. Reverse switching of surface roughness in a self-organized polydomain liquid crystal coating. *Proc. Natl. Acad. Sci. U.S.A.* **112**, 3880-3885 (2015).
7 Liu, D. & Broer, D. J. New insights into photoactivated volume generation boost surface morphing in liquid crystal coatings. *Nat. Commun.* **6**, 8334 (2015).
8 Sidorenko, A., Krupenkin, T., Taylor, A., Fratzl, P. & Aizenberg, J. Reversible switching of hydrogel-actuated nanostructures into complex micropatterns. *Science* **315**, 487-490 (2007).
9 He, X. M. *et al.* Synthetic homeostatic materials with chemo-mechano-chemical self-regulation. *Nature* **487**, 214-218 (2012).

10 Aizenberg, J., Hatton, B., Yao, X., Aizenberg, M. & Wang, W. Dynamic and switchable slippery surfaces. US9683197B2 (2017).
11 Khalil, K. S., Mahmoudi, S. R., Abu-dheir, N. & Varanasi, K. K. Active surfaces: Ferrofluid-impregnated surfaces for active manipulation of droplets. *Appl. Phys. Lett.* **105** (2014).
12 Tian, D. *et al.* Fast responsive and controllable liquid transport on a magnetic fluid/nanoarray composite interface. *ACS Nano* **10**, 6220-6226 (2016).
13 Irajizad, P., Hasnain, M., Farokhnia, N., Sajadi, S. M. & Ghasemi, H. Magnetic slippery extreme icephobic surfaces. *Nat. Commun.* **7**, 13395 (2016).
14 Xia, F. & Jiang, L. Bio-inspired, smart, multiscale interfacial materials. *Adv. Mater.* **20**, 2842-2858 (2008).
15 Rosensweig, R. E. *Ferrohydrodynamics*. (Dover Publications, 1997).
16 Rosensweig, R. E. Magnetic Fluids. *Sci Am* **247**, 136 (1982).
17 Odenbach, S. in *Lecture Notes in Physics: Colloidal Magnetic Fluids: Basics, Development and Application of Ferrofluids* (Springer-Verlag Berlin Heidelberg, 2009).
18 Timonen, J. V. I., Latikka, M., Leibler, L., Ras, R. H. A. & Ikkala, O. Switchable static and dynamic self-assembly of magnetic droplets on superhydrophobic surfaces. *Science* **341**, 253-257 (2013).
19 Torres-Diaz, I. & Rinaldi, C. Recent progress in ferrofluids research: novel applications of magnetically controllable and tunable fluids. *Soft Matter* **10**, 8584-8602 (2014).
20 Timonen, J. V. I., Demirörs, A. F. & Grzybowski, B. A. Magnetofluidic tweezing of nonmagnetic colloids. *Adv. Mater.* **28**, 3453-3459 (2016).
21 Yao, X. *et al.* Adaptive fluid-infused porous films with tunable transparency and wettability. *Nat Mater* **12**, 529-534 (2013).
22 Schellenberger, F. *et al.* Direct observation of drops on slippery lubricant-infused surfaces. *Soft Matter* **11**, 7617-7626 (2015).
23 Parsegian, V. A. *Van der Waals Forces : a Handbook for Biologists, Chemists, Engineers, and Physicists*. (Cambridge University Press, 2006).
24 Israelachvili, J. N. *Intermolecular and Surface Forces*. 3rd edn, (Academic Press, 2011).
25 Reiter, G. *et al.* Thin film instability induced by long-range forces. *Langmuir* **15**, 2551-2558 (1999).
26 Hatch, A., Kamholz, A. E., Holman, G., Yager, P. & Bohringer, K. F. A ferrofluidic magnetic micropump. *J. Microelectromech. Syst.* **10**, 215-221 (2001).
27 Pokroy, B., Kang, S. H., Mahadevan, L. & Aizenberg, J. Self-organization of a mesoscale bristle into ordered, hierarchical helical assemblies. *Science* **323**, 237-240 (2009).
28 McKeon, B. J., Sharma, A. S. & Jacobi, I. Experimental manipulation of wall turbulence: A systems approach. *Phys. Fluids* **25** (2013).
29 Park, K.-C. *et al.* Condensation on slippery asymmetric bumps. *Nature* **531**, 78-82 (2016).
30 Pamme, N. Magnetism and microfluidics. *Lab Chip* **6**, 24-38 (2006).
31 Verho, T. *et al.* Reversible switching between superhydrophobic states on a hierarchically structured surface. *Proc. Natl. Acad. Sci. U.S.A.* **109**, 10210-10213 (2012).
32 Epstein, A. K., Wong, T. S., Belisle, R. A., Boggs, E. M. & Aizenberg, J. Liquid-infused structured surfaces with exceptional anti-biofouling performance. *Proc. Natl. Acad. Sci. U.S.A.* **109**, 13182-13187 (2012).